Co-development of a cyclone family and an atmospheric river over the North Atlantic: a synoptic evolution with associated moisture transports

Co-development of a cyclone family and an atmospheric river over the North Atlantic: a synoptic evolution with associated moisture transports

Jun-Ichi Yano[1] and Oscar Martínez-Alvarado[2,3]

[1]*CNRM, UMR3589 (CNRS), Météo–France, Toulouse Cedex, France*
[2]*National Centre for Atmospheric Science, University of Reading, UK*
[3]*Department of Meteorology, University of Reading, UK*

Introduction

The passage of synoptic-scale cyclones over the British Isles and Europe can lead to extreme rainfall, which can then lead to flooding (e.g. Huntingford *et al*., 2014). A prototype picture of these synoptic-scale cyclones is provided by the concept of a cyclone family, originally introduced by the Bergen School (Bjerknes and Solberg, 1922): a series of cyclones forming in sequence along the same surface polar front. Interest in the cyclone family has been recently renewed (Priestley *et al*., 2020), partially due to their association with damaging events (*cf*. Dacre and Pinto, 2020).

As another potential cause of extreme rainfall and natural disasters, atmospheric rivers (e.g. Lavers *et al*., 2011; Lavers and Villarini, 2013) are also increasingly drawing attention. These features, originally identified by satellite imagery analysis (Newell *et al*., 1992), are filaments of high moisture transport in the atmosphere. These filamentary structures often stretch from the tropics to higher latitudes. Arguably, the concept of the atmospheric river is already implicitly embedded in the original prototype picture of Bjerknes and Solberg (1922), in which a low-level jet along the cold front extends polewards from the subtropics (*cf*. their figs. 11 and 12, also reproduced as e.g. Figure 1 by Dacre and Pinto, 2020) as argued by Browning (2018). The present paper pursues this perspective of the atmospheric river as an integrated part of synoptic-scale weather systems. The adopted approach here may best be understood as a response to a hypothetical question of how the Bergen school would have presented atmospheric rivers if good measurements of the moisture field had been in their hands: we closely follow the evolution of the moisture field in association with the evolution of the synoptic-scale cyclone systems from this perspective. Also following the canonical picture of Bjerknes and Solberg (1922), we take a case with a well-defined synoptic cyclone family that developed over the North Atlantic during September 2018. An extensive atmospheric river also formed in association with this cyclone family.

The close link between both features has already been widely recognised (*cf*. Ralph *et al*., 2020). The current understanding of the synoptic-scale dynamics associated with atmospheric rivers is reviewed in Sodemann *et al*. (2020). Studies of the atmospheric rivers from the perspective of synoptic-scale dynamics are found, for example, in Ralph *et al*. (2004) and Dacre *et al*. (2015, 2019). However, existing studies focus more on the statistically averaged synoptic state associated with atmospheric rivers and the associated long-duration heavy precipitation (e.g. Fish *et al*., 2019; Moore *et al*., 2021). The present study is more descriptive, yet direct: it follows the synoptic evolution of the moisture and the surface pressure fields side by side so that we can examine the evolution of the atmospheric rivers as a part of the synoptic-scale weather systems. Furthermore, basic synoptic-scale processes associated with the atmospheric river are inferred by evaluating the associated timescales.

The present paper avoids statistical tools introduced in many studies of atmospheric rivers. Especially, rather than adopting standard detection methods, which reduce the moisture field into 1 or 0 depending on whether or not it belongs to an atmospheric river (e.g. Lavers and Villarini, 2013; Xu *et al*., 2020), this study examines the continuous distribution of the moisture field to find how atmospheric rivers emerge and dissolve under the evolution of the moisture field. This analysis is further extended to a period before the event to examine how the moisture field has evolved towards this atmospheric river event from the earlier states; hence, the event is better characterised by comparing it with the evolution of the moisture field during the non-atmospheric river period.

In the present paper, we adopt the morphological picture originally proposed by Newell *et al*. (1992) and summarised by fig. 1 of Dettinger *et al*. (2015) for the atmospheric river: a stream-like structure of high moisture transport stretching from the tropics to higher latitudes. By following this picture, we identify the atmospheric river as a well-defined horizontal stretch, taking the form of a narrow strip in the moisture field. This picture may be contrasted with more recent studies, especially in association with extreme events (e.g. Lavers and Villarini, 2013), that apply the strict thresholds for identifications: as the threshold increases, the atmospheric river defined by the closed contour with the given threshold also decreases in length.

An alternative synoptic-scale perspective to interpret the atmospheric river is as a backward extrapolation of the warm conveyor belt (WCB), which is an upward moisture transport along the cold front interface (*cf*. fig. 4d of Dacre *et al*., 2015). The low-level jet leading to the WCB is often associated with a high moisture field, which may even be considered a definition of the atmospheric river (e.g. Browning, 2018). Conversely, an atmospheric river is expected to typically lead to a WCB (*cf*. fig. 1 of Dettinger *et al*., 2015). However, when an atmospheric river is formed in association with a cyclone family, as in the present study, a more complex picture emerges.

We proceed as follows. A morphological description in the first half of the paper

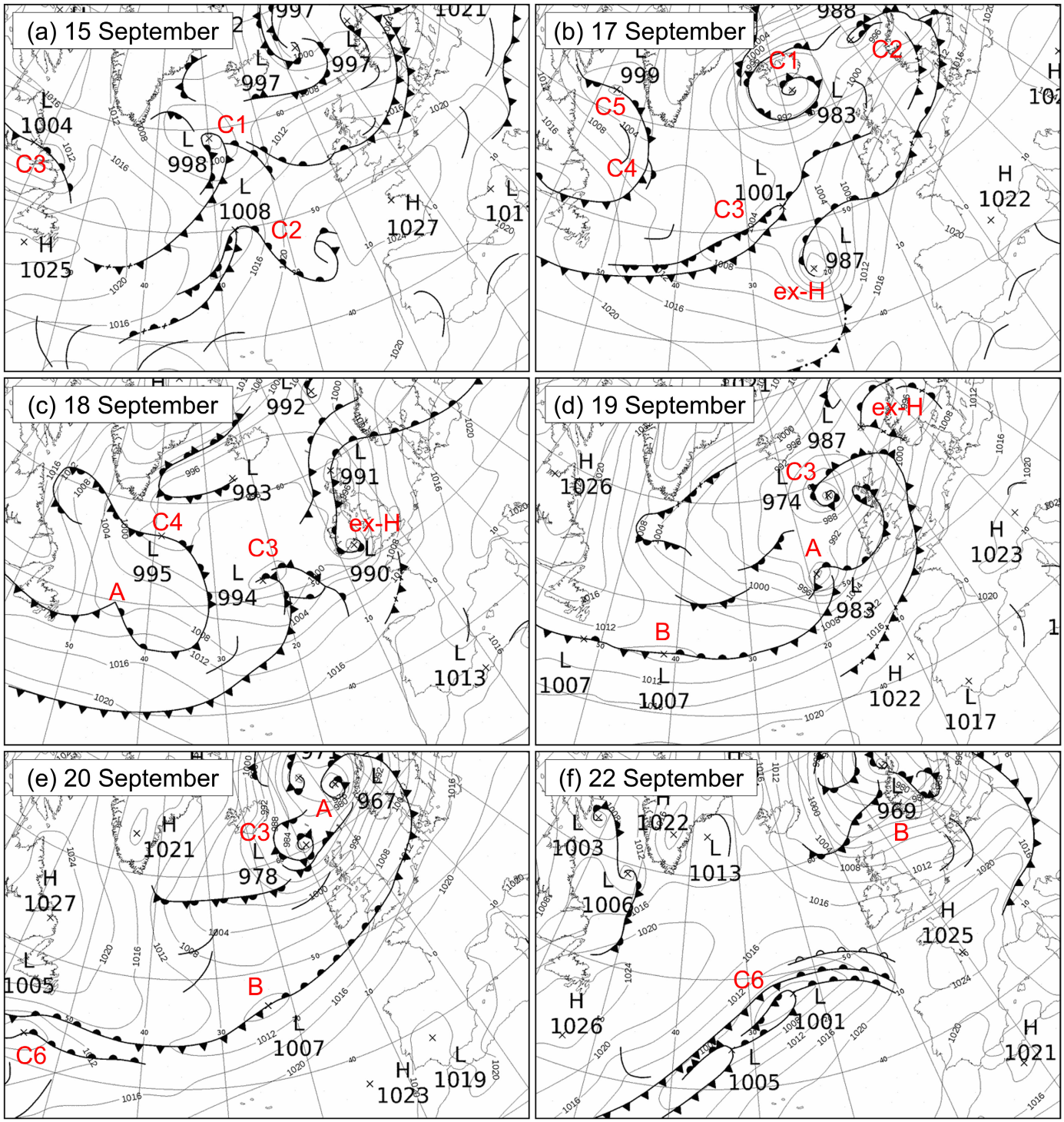

Figure 1. Annotated Met Office analysis charts at 0000 UTC on (a) 15, (b) 17, (c) 18, (d) 19, (e) 20, and (f) 22 September 2018 as indicated in each panel, also showing the positions of North Atlantic cyclones during this period. The analysis charts mark the sea level pressure (hPa), front positions, and extrema of the surface pressures with the maximum and minimum marked by H and L, respectively. The pressure contour intervals are 4hPa. Analysis charts are Crown copyright.

reveals the synoptic-scale dynamics controlling the evolution of atmospheric rivers. The last half of the paper quantifies the timescales associated with the synoptic-scale dynamics controlling atmospheric rivers: atmospheric rivers evolve with a relatively short timescale, less than 24h, in association with vertical transport. The quantification here, also following the spirit of the Bergen school to understand the weather charts from a physical basis, complements the moisture budget studies by, for example, Dacre *et al*. (2015, 2019, 2023) and Guan *et al*. (2020).

Data and methods

The weather charts presented are based on the 6-hourly Met Office analysis, which is produced operationally by forecasters using a range of products including the output of the Met Office Unified Model and the forecasters' expertise. The locations of the cyclones occurring in the North Atlantic during the period of the study are assessed manually, based on surface pressure minima, using 6-hourly Met Office analysis charts.

Furthermore, ERA5 (Hersbach *et al*., 2020), the fifth-generation reanalysis produced by the European Centre for Medium-range Weather Forecasts, provides mean sea level pressure, total column water vapour (TCWV), the vertically integrated water vapour trans-

port (IVT) and total column water vapour convergence (TCVC), provided as vertically integrated moisture flux divergence. All these single-level fields were retrieved every 6h starting on 0000 UTC 1 September 2018 and throughout that month on a regular $0.25^{\circ} \times 0.25^{\circ}$ longitude–latitude grid.

The present study, by following a commonly accepted custom (Rutz *et al*., 2015), uses the IVT value of 250kgm^{-1}s^{-1} as a marker to visually identify a stream-like structure of high moisture transport stretching from the tropics to higher latitudes as an atmospheric river, *but not* as means of defining it.

Cyclone family event: synoptic description

During the period, 15–20 September 2018, a series of nine cyclones developed in close sequence over the North Atlantic, including post-tropical cyclone *Helene*, and storms *Ali* and *Bronagh*, the first two storms named by the UK Met Office in the 2018–2019 season. The last three cyclones of the series formed a cyclone family. This study period is that of intensive active cyclone activity in the North Atlantic (Gentile *et al*., 2021). In particular, Storm *Bronagh* caused localised flooding in parts of England and Wales (Cuckow *et al*., 2022).

Two cyclones (C1, C2) found over the Atlantic on 14 September lead this series of cyclones, and a third cyclone (C3) is forming behind just off Newfoundland. As cyclones C1 and C2 move farther to the middle of the Atlantic, cyclone C3 remains over Newfoundland on 15 September (Figure 1a). By 17 September (Figure 1b), cyclone C1 has moved northeast towards Iceland, cyclone C2 has passed just north of the UK and cyclone C3 has moved towards the middle of the Atlantic. A long-stretched cold front crossing the Atlantic in association with cyclone C3 may also be noted (Figure 1). Such an extended frontal structure is considered a precondition for forming a cyclone family. Note, however, that no more cyclones develop along this trailing cold front immediately behind. At this point, post-tropical cyclone *Helene*, which underwent extratropical transition on 16 September, is located just south of cyclone C3 propagating towards the UK (Figure 1b). Post-tropical cyclone *Helene* then follows behind the three cyclones, C1–C3.

A separate well-defined extended frontal structure initially associated with cyclones C4 and C5 between Greenland and Newfoundland (Figure 1b) takes another 3 days to fully develop between 18 and 20 September (Figures 1c–e). As the frontal structure develops, the cyclone family that closely follows the canonical picture by Bjerknes and Solberg (1922) initiates with cyclone *Ali* (Figure 1c) and can be fully identified on 20 September (Figure 1e): an extensive cold front crosses the whole Atlantic and further stretches to Scandinavia, crossing over the UK. Along this front, three cyclones are aligned to form a well-defined cyclone family: *Ali* (A), *Bronagh* (B) and cyclone C6. However, this cyclone family is not sustained long: as *Bronagh* crosses over the Atlantic during 19–21 September, following *Ali*, only the last cyclone, C6, is found over the Atlantic on 22 September (Figure 1f). With no cyclone following behind, this cyclone family event, initiated from a close sequence of cyclones, ends.

IVT field: preformation stage of the atmospheric river

A well-defined atmospheric river formed in association with the cyclone family presented in the last section. In the following three sections, we present the evolution of the IVT field leading to these atmospheric river events, its formation stage and how it ended. We examine the evolution of the IVT field for a more extended period, especially because the description of non-atmospheric river state provides a good point of reference to see how an atmospheric river state can be contrasted against a '*normal*' state. It soon becomes clear that the IVT evolution hardly consists of those two distinguished states in a dichotomous manner. Rather, under continuous evolution, an atmospheric river gradually emerges and then dissolves without any well-defined transitions: an atmospheric river period cannot be defined in any strict manner, unless a predefined threshold, single or a set, is imposed specifically, as is the case with many other atmospheric phenomena. Specifically, we will often identify a chain of high IVT patches around cyclones, which is not dissimilar to an atmospheric river, but the '*flow*' is not as homogeneous as a river must be. For this reason, when we judge the strip of high IVT is not long enough to call it a '*river*', we simply call it a '*stretch*', and furthermore, if not narrow enough, a '*patch*'.

The formation of the well-defined extensive atmospheric river over the Atlantic during 18–20 September is proceeded by a cycle of '*active*' and '*break*' phases of atmospheric rivers associated with a gradual build-up of IVT over the North Atlantic. The beginning of this full cycle can be identified by a weak atmospheric river extending from the middle of the Atlantic into the Norwegian Sea and as north as Svalbard, '*flowing*' along the southeast side of a cyclone over Iceland, on 1 September (Figure 2a). Another atmospheric river flowing towards Quebec along the North American East Coast is identified, turning around the Gulf of Mexico along the Azores high and originating from the subtropical Atlantic. The first atmospheric river largely dissipates by 4 September (Figure 2b), whereas the second southern counterpart is still well maintained. On 9 September, a relatively weak stretch of IVT, less than 500kgm^{-1}s^{-1}, is identified over the UK in association with a cyclone centred south of Iceland (not shown).

By 10 September, a well-defined atmospheric river is formed around the Azores high and extending well into the subtropics with four high IVT patches, three of them at low latitudes associated with tropical cyclones and one in the midlatitudes associated with an extratropical low-pressure system (Figure 2c). By 13 September, this strong atmospheric river dissipates into a stretch of weak IVT (Figure 2d). In the following days, this weak IVT stretch remains relatively stationary, as maintained by the circulation induced by a relatively stationary low over Iceland. On 14 September, the weak IVT stretch becomes the leading edge of the atmospheric river that merges with a high IVT induced by the circulation due to cyclone C2 and Tropical Storm *Helene* at its southern edge. This marks the beginning of the cyclone family event of 18–20 September.

Atmospheric river: formation and dissolution

A possible contribution from the tropics in forming the atmospheric river during 18–20 September is from Tropical Storm *Helene*: on 15 September (Figure 3a), we find that *Helene* effectively constitutes the southwest edge of the atmospheric river associated with cyclone C2. Another structure with high IVT is also seen moving from the west over North America on 15 September along with cyclone C3 (Figure 3a). In mean time, *Helene* undergoes extratropical transition as it travels north and becomes an extratropical system on 16 September. These two separate segments of high IVT, associated with post-tropical cyclone *Helene*, C2 and C3, merge together on 17 September (Figure 3b).

This merger forms a long atmospheric river across the Atlantic, also incorporating the IVT induced by the first cyclone family cyclone, *Ali*. On 18 September (Figure 3c), a high IVT signal crossing the Atlantic further continues backwards to North America, then farther back to the subtropical Atlantic by following the flow of the Azores high. Morphologically speaking, the atmospheric river formed here, consistent with the canonical picture originally presented by Newell *et al*. (1992), appears to represent a moisture transport route from the tropics to the midlatitudes, and in the most prominent manner over the 22-day analysis period.

The first and last day that a well-defined atmospheric river can be connected to easterly flow in the tropics is on 18

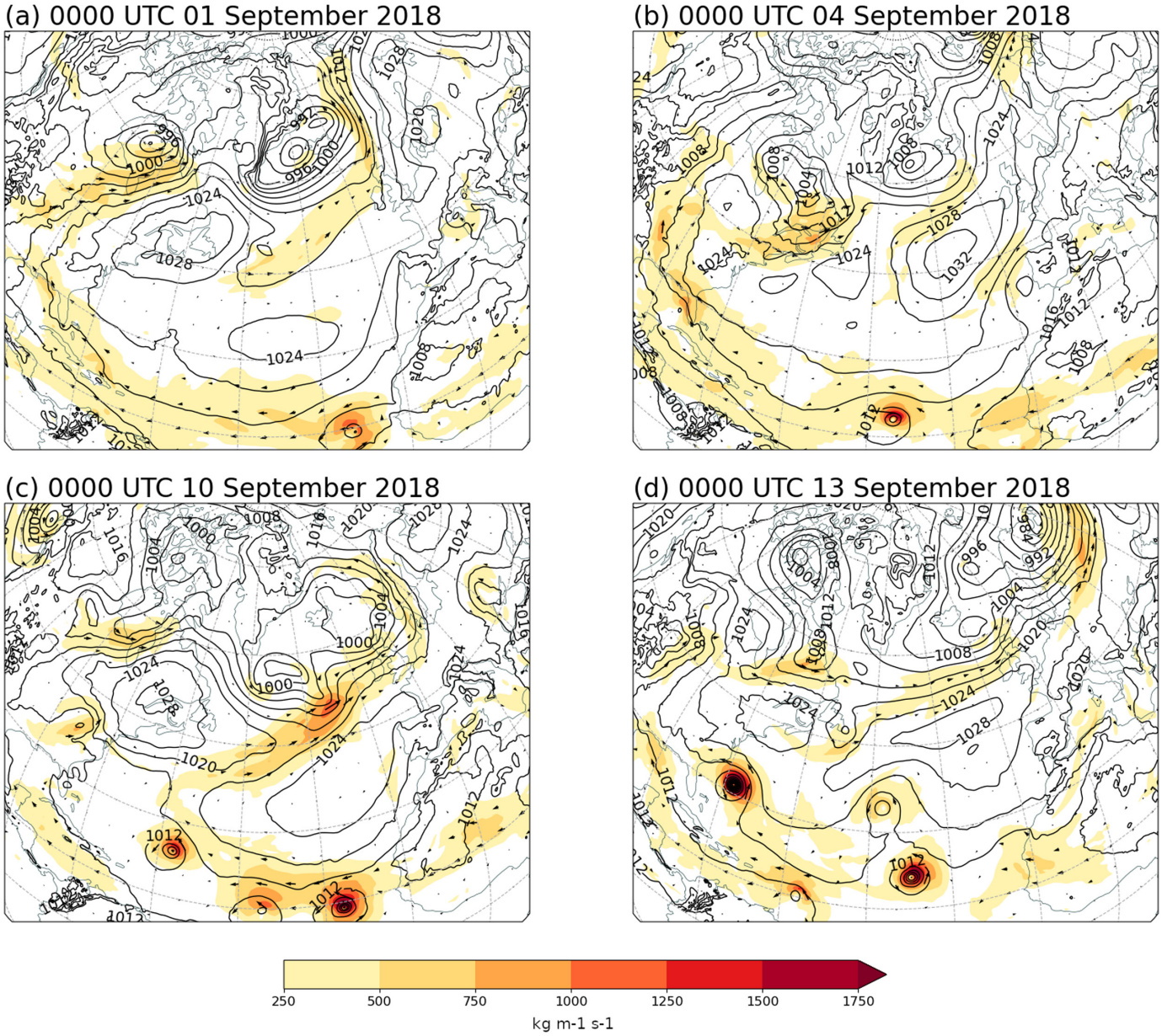

Figure 2. Vertically–integrated vapour transport (IVT, kgm^{-1}s^{-1}: shading) and mean sea level pressure (black contours with intervals of 4hPa) at 0000 UTC on (a) 1, (b) 4, (c) 10, and (d) 13 September 2018 as indicated in each panel, also showing the positions of North Atlantic cyclones during the period. Short vectors further indicate the directions of the IVTs.

September, with the three cyclones, post-tropical cyclone *Helene*, C3, and *Ali*, aligning together in the mid-latitudes (Figure 3c). The atmospheric river on this day stretches continuously around the Azores high from the subtropics, although relatively weak in magnitude. On 19 September (Figure 3d), this continuous long stretch of the atmospheric river is already disrupted by high IVT patches associated with the three cyclones, *Ali* (A), *Bronagh* (B) and cyclone C6. From this point, the extratropical atmospheric river, over the north side of the Azores high, begins to be detached from the southern counterpart. Yet, the remaining extratropical atmospheric river is strongest in magnitude on 20 September (Figure 3e).

The canonical atmospheric river identified during 18–20 September breaks down immediately afterwards: on 21 September, we find that two high IVT stretches in association with two secondary cyclones (not shown). On 22 September (Figure 3f), the atmospheric river structure identified over the previous few days is no longer recognisable. We only see three isolated patches of high IVT in association with three cyclones on the chart.

Morphological interpretations

The formation process of the atmospheric river during 18–20 September can be morphologically interpreted in various manners, although none of them is without problem. First, it can be interpreted that the climatological presence of the Azores high maintains a circulation along which the atmospheric river flows. However, this interpretation can be misleading, because this atmospheric river is maintained only over 3 days.

It may be also noted that this atmospheric river, formed along the cyclone family, also aligns well with an equally well-stretched cold front on 20 September, as seen from Figures 1(e) and 3(e). However, it is not always the case that an atmospheric river is formed along a well-stretched cold front: no atmospheric river is identified along the cold front stretched from cyclone C3 in Figure 3(b): a strip of high ITV in the proximity is rather associated with post-tropical cyclone *Helene*.

Alternatively, it may be argued that *Helene* provided the necessary moisture source for forming an atmospheric river by following the view of Krichak *et al.* (2004, 2006, 2015). A hypothesis of the tropical cyclone origin of this atmospheric river is, however, inconsistent with the fact that reasonably long stretches of high IVT are already identified

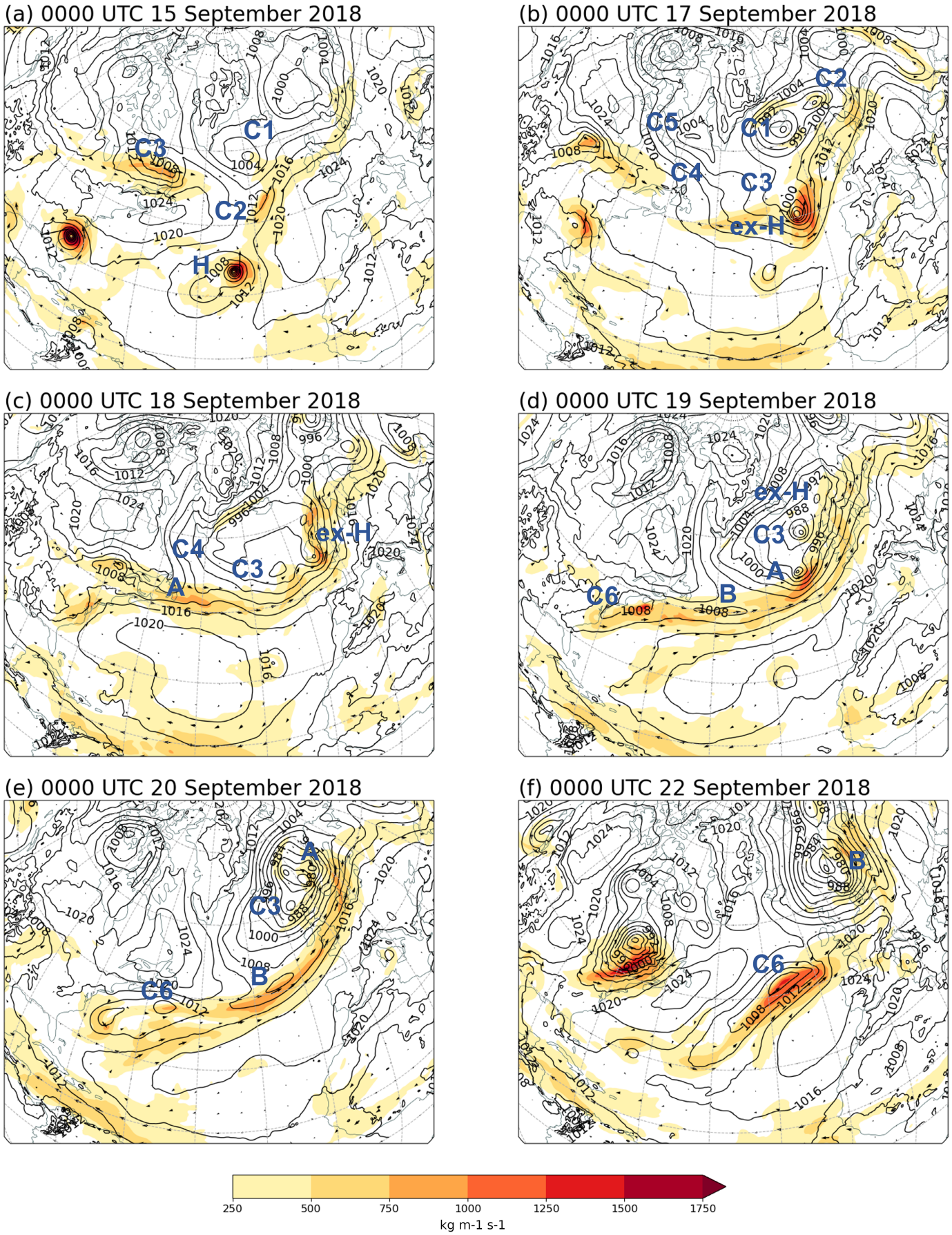

Figure 3. Vertically–integrated vapour transport (IVT, kgm^{-1}s^{-1}: shading) and mean sea level pressure (black contours with intervals of 4hPa) at 0000 UTC on (a) 15, (b) 17, (c) 18, (d) 19, (e) 20, and (f) 22 September 2018 as indicated in each panel. In the same format as for Figure 2.

RMetS Royal Meteorological Society

on 15 September (Figure 3a), associated with C2 and to a lesser extent with C1, ahead of the high IVT associated with Tropical Storm *Helene*. Inspection of 6-hourly plots of IVT reveals that, more precisely, Tropical Storm *Helene* merges into this pre-existing stretch of an atmospheric river, although the IVT field of 18 September (Figure 3c) may give an impression that post–tropical cyclone *Helene* is a source of the atmospheric river.

As seen from the morphological description of the IVT field so far, atmospheric river structures in the midlatitudes are formed locally by following the evolution of the synoptic-scale cyclones along their southern portions: advection of moisture by the synoptic-scale flows drives the evolution of atmospheric rivers. Under the intermittent evolution of midlatitude atmospheric rivers, a canonical form with high IVT stretching continuously around a subtropical Azores high may be realised, but only over limited periods: each realisation lasts only between 1 and 3 days over the 22-day period considered, too short to transport the tropical moisture to the midlatitudes, as going to be evaluated in the next section.

Water vapour transport speed

Now, how efficiently does the atmospheric river, analysed in the previous sections, work as a moisture transport route of a purely advective process? Here, the water vapour is transported horizontally as the air mass that contains the water vapour moves with the wind velocity. Amount of the total water vapour contained in a single atmospheric column from the surface to the top of the atmosphere is measured by the total column water vapour (TCWV: Equation 1a of Box 1). Conceptually, the water vapour is transported by moving this atmospheric column by a certain speed (water vapour transport speed), u, so that the observed integrated vapour transport (IVT) is realised, that is,

$$u = \mathrm{IVT} / \mathrm{TCWV} \tag{2}$$

Note that it measures a purely advective process of the atmospheric river. In reality, the water vapour is transported with different wind speeds at different heights. The water vapour transport speed, u, is obtained by vertically averaging the wind speed weighted by the water vapour, as seen in the above definition (2).

By taking typical values of IVT and TCWV for atmospheric rivers, we obtain a value:

$$u \sim \frac{250\mathrm{kgm^{-1}s^{-1}}}{25\mathrm{kgm^{-2}}} = 10\mathrm{ms^{-1}} \tag{3}$$

This value is fairly comparable to typical propagation speeds of synoptic-scale cyclones (e.g. Bjerknes and Solberg, 1922). Note that the moisture column moves about 10^3km over a day with a transport speed of 10ms^{-1}; thus, about 10 days are required to transport moisture from the tropics to a midlatitude. It is not a coincidence that 10ms^{-1} also corresponds to a typical synoptic-scale wind speed: the water vapour is transported along the atmospheric river by synoptic-scale winds, leading to extensive horizontal transport.

Here, the water vapour transport speed, u, as defined above (Equation 2) is not merely a means of estimating the order of magnitude of the transport speed, as just presented: the transport speed, u, can be evaluated at every horizontal point to provide the transport speed of TCWV, that exactly leads to the observed IVT. This distribution is shown in Figure 4: atmospheric rivers are marked by the regions of the transport speed, u, above 10ms^{-1}, and u is systematically smaller outside the atmospheric rivers. Moreover, the transport speed, u, can even exceed 30ms^{-1} inside cyclones, where the water vapour is transported in a cyclonic manner by following the flow inside the cyclone, rather than contributing to a long-range transport. Thus, u=10ms^{-1} adopted for estimating the transport timescale (Equation 3) is not much of an underestimation.

Total column water vapour convergence (TCVC)

Yet, the idea that atmospheric rivers simply transport water over very long distances, purely by horizontal transport as diagnosed in the last section, could be misleading: moisture is also transported vertically, often associated with warm conveyor belts. Here, the vertical transport itself merely changes the vertical distribution of the moisture in a given atmospheric column, without changing TCWV. An important consequence of the vertical transport is that the moisture is either gathered to or dispersed from a given atmospheric column by the low-level convergence and divergence, respectively, in association with the upward and downward motion of the moist air from and to the lower level. To assess the extent of such an effect of the vertical transport of moisture, we now examine the total convergence of water vapour integrated over the atmospheric column (total column water vapour convergence, TCVC: Equation 1c in Box 1). Here, the convergence rate, measuring a rate at which a physical quantity merges to a single horizontal point, is evaluated for the water vapour with a vertical integral so that a vertically accumulated effect can be assessed.

The most straightforward speculation, by following a local generation process of atmospheric rivers in association with midlatitude cyclones, is that the moisture distribution of atmospheric rivers is maintained by local convergence of moisture along the low-level jet associated with the cold front (*cf.* fig. 4c of Dacre *et al*., 2015). Yet, even a quick glance of the TCVC field betrays this speculation (Figure 5): a wave-like, yet highly irregular interchange of moisture convergence and divergence is typically found along an atmospheric river identified by IVT.

Note that those moisture convergence and divergence are, respectively, associated with low-level convergence and divergence of the flow due to the fact that most of the moisture is found in the lower troposphere (below 700hPa). Thus, these two different convergence and divergence processes can be considered equivalent qualitatively, as we consider in the following.

A relative phase between the TCVC and the surface pressure presents certain consistencies with what is expected from the omega equation, an equation that diagnoses the convergence for the synoptic-scale flow in good approximations, with a tendency of low-level convergence and divergence ahead and behind a cyclone (*cf.* Holton and Hakim, 2013, see especially their fig. 6.14). Referring to the schematics given by fig. 7 of Dacre *et al*. (2019), we further interpret that they are associated with the warm conveyor belts (WCBs) and the dry intrusions, respectively. However, this correspondence is rather crude, and TCVC also contains much smaller scale structures than the surface pressure, partially due to the fact that the divergence field is related to the second-order horizontal derivatives of the pressure through the vorticity equation. Also, those wave-like patterns occur far away from the cyclone centres; thus,

Box 1.

TCWV, IVT and TCVC are defined, respectively, as:

$$\mathrm{TCWV} = \frac{1}{g}\int_0^{p_s} q\,dp \tag{1a}$$

$$\mathrm{IVT} = \frac{1}{g}\left|\int_0^{p_s} q\mathbf{u}_H\,dp\right| \tag{1b}$$

$$\mathrm{TCVC} = -\frac{1}{g}\int_0^{p_s} \nabla_H \cdot q\mathbf{u}_H\,dp \tag{1c}$$

in terms of g the acceleration due to gravity, p the pressure, q the specific humidity, $\mathbf{u}_H$ the horizontal wind velocity and $-\nabla_H \cdot q\mathbf{u}_H$ the convergence rate of the moisture at a given pressure level. Note that all the above integrals are performed from the surface to the top of atmosphere, although the contributions from above the tropopause are negligible in practice.

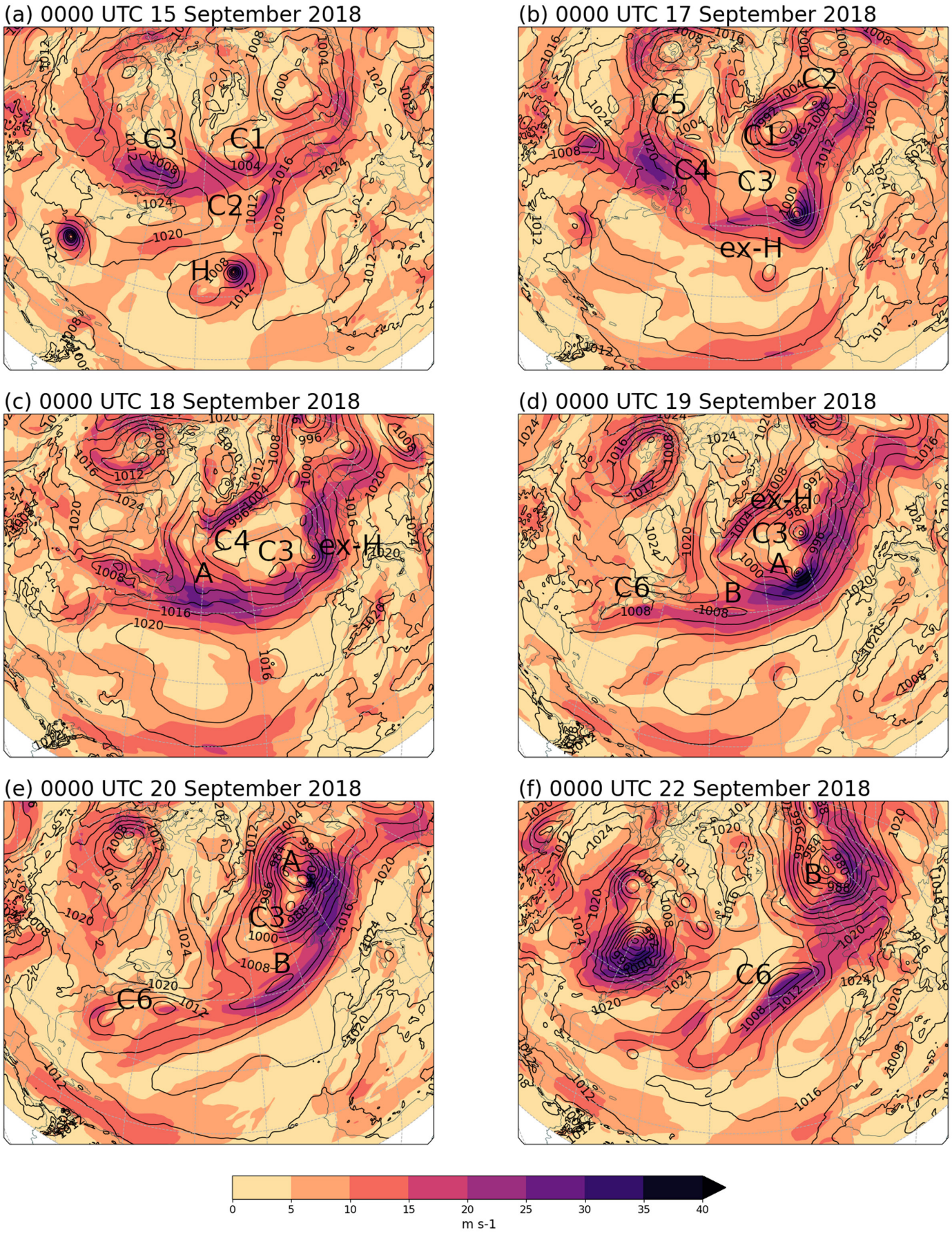

Figure 4. Distribution of the water–vapour transport speed, u, on (a) 15, (b) 17, (c) 18, (d) 19, (e) 20, and (f) 22 September 2018.

not all convergence regions are necessarily associated with WCBs (*cf.* fig. 4d of Dacre *et al.*, 2015).

Here, as moisture is transported horizontally along an atmospheric river, the atmospheric column experiences depletion and supply of the moisture associated with divergence and convergence: the atmospheric river is hardly a simple horizontal

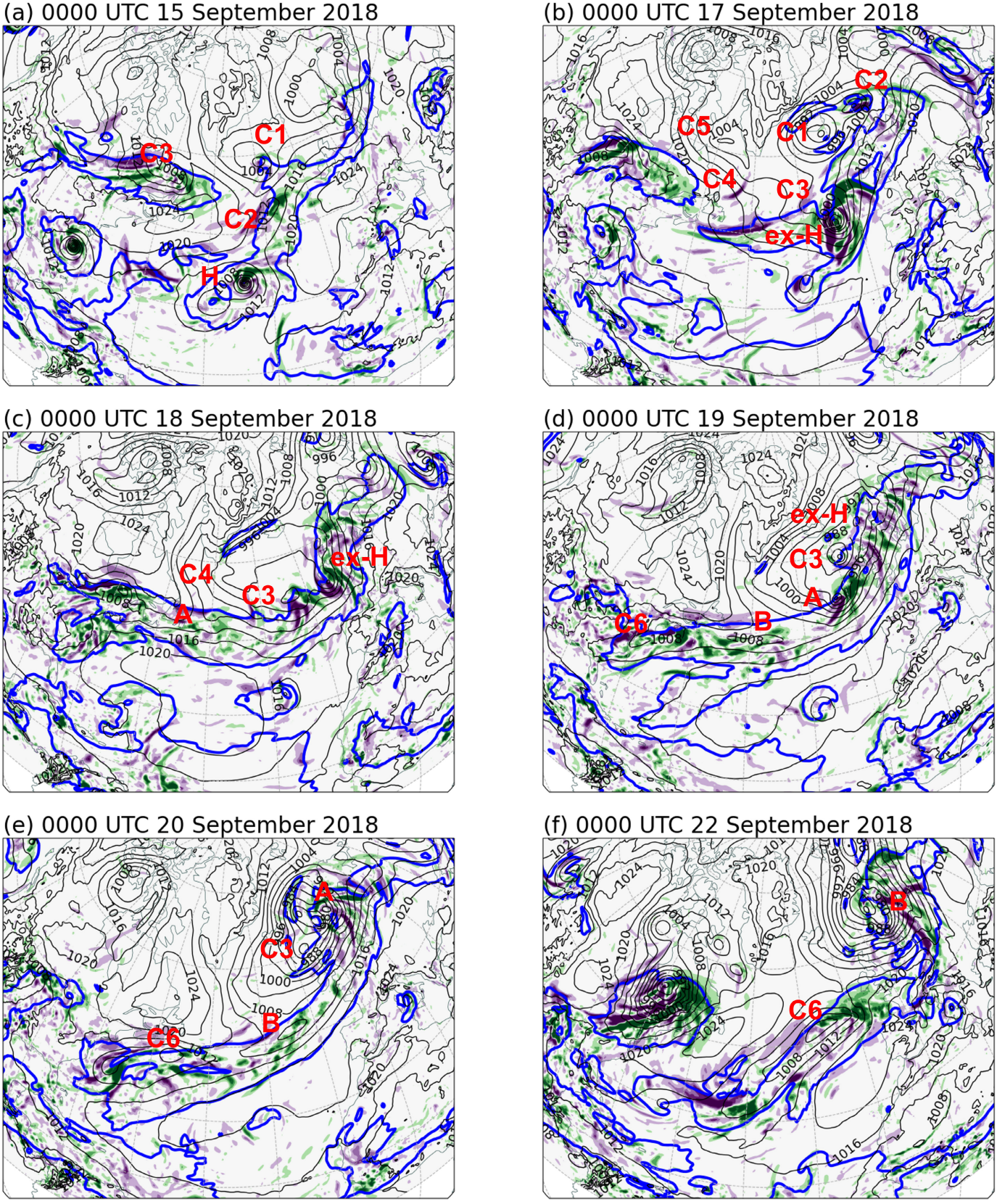

Figure 5. Total column water–vapour convergence (TCVC, $kgm^{-2}s^{-1}$: shading), mean sea level pressure (black contours with intervals of 4hPa), and $250kgm^{-1}s^{-1}$ IVT contour (blue) at 0000 UTC on (a) 15, (b) 17, (c) 18, (d) 19, (e) 20, and (f) 22 September 2018 as indicated in each panel, also showing the positions of North Atlantic cyclones (cf. Figure 1).

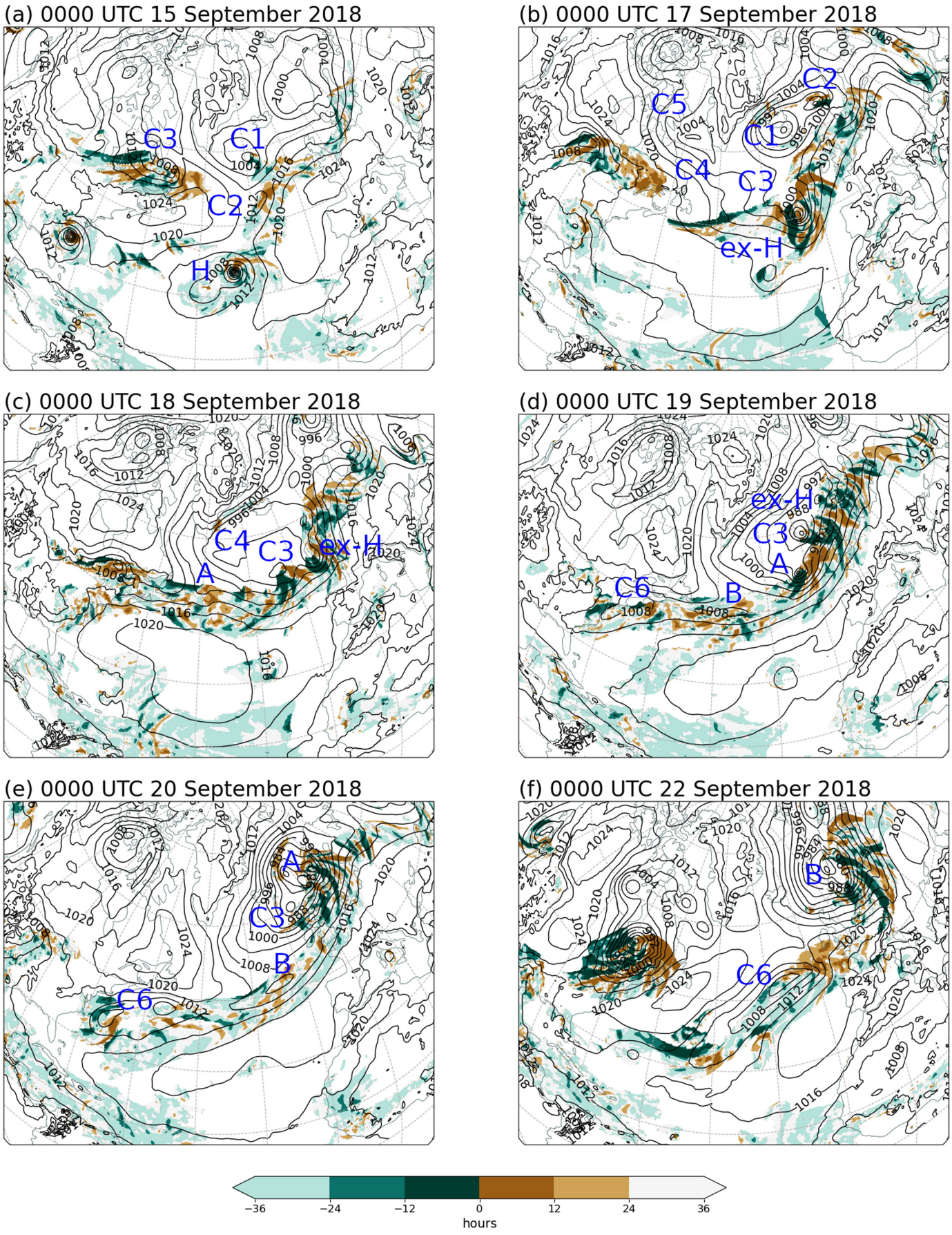

Figure 6. Moisture recycling time (τ, hours: shading) and mean sea level pressure (black contours with intervals of 4hPa) at 0000 UTC on (a) 15, (b) 17, (c) 18, (d) 19, (e) 20, and (f) 22 September 2018 as indicated in each panel, also showing the positions of North Atlantic cyclones during the period (cf. Figure 1).

flow of moisture but also associated with extensive recycling of moisture associated with a divergent flow. Furthermore, convergence is associated with upward transport of moisture followed by condensation and precipitation: a substantial fraction of moisture is lost along the atmospheric river in this manner. The lost moisture is, in turn, locally resupplied by surface evaporation, especially over the feeder airstreams for the moisture converging into WCBs (Dacre *et al*., 2015, 2019).

The time, τ, required for the recycling of moisture associated with the vertical transport may be measured by:

$$\tau = \mathrm{TCWV} / \mathrm{TCVC} \tag{4}$$

More precisely, $1/\tau$ is a fractional rate that TCWV is changed by TCVC, in association with the vertical transport. Here, the recycling time, τ, is positive or negative depending on the sign of TCVC, that is, whether TCWV tends to increase or decrease, respectively, under moisture convergence or divergence. Over the absolute value of this time, τ, a given total water vapour (TCWV) is either doubled or depleted, respectively, by a given rate of the convergence or divergence (TCVC) of water vapour. By substituting typical values, we find:

$$\tau \sim \frac{25\,\mathrm{kg\,m^{-2}}}{2.5\times10^{-4}\,\mathrm{kg\,m^{-2}s^{-1}}} = 10^5\,\mathrm{s} \tag{5}$$

Thus, the moisture is recycled in about a day.

Figure 6 reveals that the recycling time, τ, is systematically less that 24h along atmospheric rivers in association with strong divergence and convergence, and often even less than 12h: the given timescale is so short that we cannot properly quantify the moisture transport associated with atmospheric rivers without taking into account the vertical transport as well as the associated local moisture resupplies. Also note that the recycling time, τ, is substantially longer away from the high IVT regions: strong divergences and convergences of moisture characterise the atmospheric rivers. The analysis here generalises the moisture budget analysis focused on cyclones by Dacre *et al*. (2015, 2019) to all the way along atmospheric rivers with a much simpler single diagnosis (Equation 4) and effectively concludes the same, that is, importance of local moisture supply.

Conclusions

The co-development of a cyclone family and an extensive atmospheric river across the North Atlantic in September 2018 has been presented. A particular case with a well-defined cyclone family linked to an atmospheric river has been chosen for elucidating the characteristics of the co-development well. A direct examination of the evolution of both the surface pressure and the moisture fields side by side has exposed that the atmospheric river actively evolves locally, driven by synoptic-scale cyclones (*cf*. Figures 1 and 3): atmospheric rivers are formed and dissolved over few day timescales by following the synoptic evolution of the weather.

The horizontal transport speed, u, of atmospheric rivers evaluated from IVT and TCWV (Equation 2) is typically about $10\,\mathrm{ms^{-1}}$, which is comparable by the order of magnitude to a typical propagation speed of synoptic-scale cyclones (see also Cuckow *et al*., 2022). In this respect, atmospheric rivers can transport moisture horizontally fairly efficiently. Yet, the synoptic-scale cyclones typically propagate slightly faster than the water vapour transport speed, thus along the coordinates moving with the cyclone centre, the atmospheric rivers tend to flow away from cyclones and be left behind: atmospheric rivers are not *direct* source of water vapour for the synoptic-scale cyclones (Dacre *et al*., 2015, 2019).

The TCVC analysis (*cf*. Equation 4 and Figure 6) suggests that the moisture is maintained by the supply of moisture over a short timescale of less than 24h by convergence and divergence along atmospheric rivers associated with synoptic-scale evolution of cyclones, as well as local supply by evaporation (Dacre *et al*., 2015, 2019). Thus, the atmospheric river does not only transport moisture from the tropics to higher latitudes purely horizontally like hydrological rivers but also transports the moisture vertically even more intensively. Furthermore, a well-defined atmospheric river stretching from the tropics to higher latitudes around a climatological subtropical high is hardly persistent, but only lasts for a few days at most: the well-defined atmospheric river breaks down before moisture can be transported from the tropics to higher latitudes along, even assuming that the transport is purely horizontal.

The present study quantifies both the transport speed and the recycling time of the moisture associated with the atmospheres with simple diagnosis formulae (Equations 2 and 4). Yet, to understand those processes better, a further analysis is required of the synoptic-scale dynamics associated with the atmospheric rivers more directly, most likely under the framework of semi-geostrophy (a higher order approximation to the quasi-geostrophy designed to describe the front dynamics; Hoskins and Bretherton, 1972), but it will be left for a future study.

Acknowledgements

Jun–Ichi Yano appreciates the discussions with Helen Dacre over last several years. She has also provided us helpful inputs in developing the present manuscript. Oscar Martínez-Alvarado's contribution was supported by the UK Natural Environment Research Council as a member of the National Centre for Atmospheric Science and as part of the '*Climate change in the Arctic – North Atlantic region and impacts on the UK*' (CANARI) programme, grant number NE/W004984/1.

Author contributions

Jun-Ichi Yano: Conceptualization; investigation; writing – original draft; methodology; writing – review and editing. **Oscar Martínez-Alvarado:** Conceptualization; methodology; visualization; writing – review and editing; formal analysis; data curation.

Data availability statement

The data that support the findings of this study are available in 6-hourly Met Office analysis at https://www.wetter3.de/archiv_ukmet_dt.html. Other data were derived from ERA5 available at the CDS API, https://cds.climate.copernicus.eu, which is managed by the Copernicus Climate Data Store. Those are more specifically: hourly data on single levels from 1940 to the present, https://doi.org/10.24381/cds.adbb2d47; hourly data on pressure levels from 1940 to the present, https://doi.org/10.24381/cds.bd0915c6.

References

Bjerknes J, **Solberg H**. 1922. Life cycle of cyclones and the polar front theory of atmospheric circulation. *Geofys. Publ.* **3**: 3–18.

Browning K. 2018. Atmospheric rivers in the U.K. *Bull. Am. Meteorol. Soc.* **99**: 1108–1109.

Cuckow S, **Dacre HF**, **Martínez-Alvarado O**. 2022. Moisture transport contributing to precipitation at the centre of Storm *Bronagh*. *Weather* **77**: 196–201.

Dacre H, **Martinez-Alvarado O**, **Hodges K**. 2023. Precipitation efficiencies in a climatology of southern ocean extratropical cyclones. *J. Geophys. Res. Atmos.* **128**: e2023JD039239.

Dacre HF, **Clark PA**, **Martinez-Alvarado O** *et al*. 2015. How do atmospheric rivers form? *Bull. Am. Meteorol. Soc.* **96**: 1243–1255.

Dacre HF, **Martínez-Alvarado O**, **Mbengue CO**. 2019. Linking atmospheric rivers and warm conveyor belt airflows. *J. Hydrometeorol.* **20**: 1183–1196.

Dacre HF, **Pinto JG**. 2020. Serial clustering of extratropical cyclones: a review of where, when and why it occurs. *NPJ Clim. Atmos. Sci.* **3**: 1–10.

Dettinger M, **Ralph FM**, **Lavers D**. 2015. Setting the stage for a global science of atmospheric rivers. *Eos* **96**. https://doi.org/10.1029/2015EO038675

Fish MA, **Wilson AM**, **Ralph FM**. 2019. Atmospheric river families: definition and associated synoptic conditions. *J. Hydrometeorol.* **20**: 2091–2108.

Gentile E, **Gray S**, **Barlow J** *et al*. 2021. The impact of atmosphere-ocean-wave coupling on the near-surface wind speed in forecasts of extratropical cyclones. *Bound.-Layer Meteorol.* **180**: 105–129.

Guan B, **Waliser D**, **Ralph F**. 2020. A multimodel evaluation of the water vapor budget in atmospheric rivers. *Ann. N. Y. Acad. Sci.* **1472**: 139–154.

Hersbach H, **Bell B**, **Berrisford P** *et al*. 2020. The ERA5 global reanalysis. *Q. J. R. Meteorol. Soc.* **146**: 1999–2049.

Holton J, **Hakim GJ**. 2013. An Introduction to Dynamic Meteorology, 5th edn. Elsevier: London.

Hoskins BJ, **Bretherton FP**. 1972. Atmospheric frontogenesis models: mathematical formulation and solution. *J. Atmos. Sci.* **29**: 11–37.

Huntingford C, **Marsh T**, **Scaife AA** *et al*. 2014. Potential influences on the United Kingdom's floods of winter 2013/14. *Nat. Clim. Chang.* **4**: 769–777.

Krichak SO, **Alpert P**, **Dayan M**. 2004. The role of atmospheric processes associated with Hurricane *Olga* in the December 2001 floods in Israel. *J. Hydrometeorol.* **5**: 1259–1270.

Krichak SO, **Alpert P**, **Dayan M**. 2006. An evalution of the role of Hurricane *Olga* (2001) in an extreme rainy event in Israel using dynamic tropopause map. *Meteorog. Atmos. Phys.* **98**: 35–53.

Krichak SO, **Barken J**, **Breitgang JS** *et al*. 2015. The role of the export of tropical moisture into midlatitudes for extreme precipitation events in the mediterranean region. *Theor. Appl. Climatol.* **121**: 499–515.

Lavers DA, **Allan RP**, **Wood EF** ***et al***. 2011. Winter floods in Britain are connected to atmospheric rivers. *Geophys. Res. Lett.* **38**: L23803.

Lavers DA, **Villarini G**. 2013. The nexus between atmospheric rivers and extreme precipitation across Europe. *Geophys. Res. Lett.* **40**: 3259–3264.

Moore BJ, **White AB**, **Gottas DJ**. 2021. Characteristics of long-duration heavy precipitation events along the West Coast of the United States. *Mon. Weather Rev.* **149**: 2255–2277.

Newell RE, **Newell NE**, **Zhu Y** *et al*. 1992. Tropospheric rivers? – A pilot study. *Geophys. Res. Lett.* **19**: 2401–2404.

Priestley M, **Dacre H**, **Shaffrey L** *et al*. 2020. The role of secondary cyclones and cyclone families for the North Atlantic storm track and clustering over western Europe. *Q. J. R. Meteorol. Soc.* **146**: 1184–1205.

Ralph FM, Dettinger MD, Waliser JJRDE (eds). 2020. Atmospheric Rivers. Springer: Dordrecht, 252pp.

Ralph FM, **Neiman PJ**, **Wick GA**. 2004. Satellite and CALJET aircraft observations of atmospheric rivers over the eastern north pacific ocean during the winter of 1997/98. *Mon. Weather Rev.* **132**: 1721–1745.

Rutz JJ, **Steenburgh WJ**, **Ralph FM**. 2015. The inland penetration of atmospheric rivers over western North America: a Lagrangian analysis. *Mon. Weather Rev.* **143**: 1924–1944.

Sodemann H, **Wernli H**, **Knippertz P** *et al*. 2020. Structure, process, and mechanism, in Atmospheric Rivers. Ralph FM, Dettinger MD, Waliser JJRDE (eds) Chap. 2. Springer: Dordrecht, pp 15–43.

Xu G, **Ma X**, **Chang P** *et al*. 2020. Image-processing-based atmospheric river tracking method version 1 (ipart-1). *Geosci. Model Dev.* **13**: 4639–4662.

Correspondence to: J.-I. Yano
jun-ichi.yano@cnrs.fr

doi: 10.1002/wea.7761